Remote Sensing of Environment 128 (2013) 44–57

Contents lists available at SciVerse ScienceDirect

Remote Sensing of Environment

journal homepage: www.elsevier.com/locate/rse

Ground-based testing of MODIS fractional snow cover in subalpine meadows and forests of the Sierra Nevada

Mark S. Raleigh [a,*], Karl Rittger [b], Courtney E. Moore [c], Brian Henn [a], James A. Lutz [d], Jessica D. Lundquist [a]

[a] Civil and Environmental Engineering, University of Washington, Box 352700, Seattle, WA 98195, USA
[b] California Institute of Technology, Jet Propulsion Laboratory, 4800 Oak Grove Drive, Pasadena, CA 91109, USA
[c] United States Department of Fish & Wildlife, 12790 Fish Hatchery Road, Leavenworth, WA 98826, USA
[d] College of the Environment, University of Washington, Box 352100, Seattle, WA 98195, USA

ARTICLE INFO

Article history:
Received 7 July 2012
Received in revised form 14 September 2012
Accepted 15 September 2012
Available online 27 October 2012

Keywords:
Snow cover
MODIS
Ground-based observations
Forests
Canopy adjustment

ABSTRACT

The Moderate Resolution Imaging Spectroradiometer (MODIS) is used widely for mapping snow cover in climate and hydrologic systems, but its accuracy is reduced in forests due to canopy obstruction. Prior validation datasets cannot quantify MODIS errors in forests, because finer-resolution passive sensors (e.g., Landsat) encounter the same canopy errors, and operational ground-based networks sample snow in clearings where snow dynamics differ from those in the forest. To assess MODIS accuracy relative to forest cover, we applied a common canopy adjustment to daily 500 m fractional snow-covered area (f_{SCA}) from the physically-based MODIS Snow-Covered Area and Grain size (MODSCAG) algorithm, and tested it at subalpine meadow and forest sites (0.25 km^2–1 km^2) in the Sierra Nevada, California during two snow seasons. 37 to 89 sensors monitored hourly ground temperature at these sites. Damped diurnal variations provided a signal for snow presence due to the insulating properties of snow, yielding daily ground-based f_{SCA} at each site. Ground-based f_{SCA} values were validated in a canopy-free area of a meadow site using time-lapse imagery and 15 m snow maps from the Advanced Spaceborne Thermal Emission and Reflection Radiometer (ASTER). Ground-based f_{SCA} had high correlation ($R^2 = 0.98$) with time-lapse data and was within 0.05 of ASTER f_{SCA}. Comparisons between MODSCAG and ground-based f_{SCA} revealed that an underestimation bias remained in the canopy-adjusted MODSCAG f_{SCA}, ranging from −0.09 to −0.22 at the meadow sites and from −0.09 to −0.37 at the forest sites. Improved canopy adjustment methods are needed for MODIS f_{SCA}.

1. Introduction

Seasonal snow cover is a critical component of the energy and water budgets of mountainous watersheds. The high albedo and low thermal conductivity of snow reduce energy absorbed by the land surface, while snowpack stores water during the winter and releases it in the spring as snowmelt. Spatial mapping of snow cover with the NASA Moderate Resolution Imaging Spectroradiometer (MODIS) (Hall et al., 2002) is convenient because of its frequent (daily) observations of snow at moderate spatial resolution (500 m). MODIS has been used to evaluate the spatial distribution of snow cover in models (Shamir & Georgakakos, 2006), to improve streamflow forecasting for reservoir operations (McGuire et al., 2006), to monitor climate change in areas with few snow observations (Bormann et al., 2012), and to reconstruct spatial distributions of snow water equivalent (SWE) (Homan et al., 2010; Rice et al., 2011; Rittger et al., 2011).

However, numerous factors limit the availability and accuracy of MODIS imagery, including cloud cover, large sensor view zenith angles (>30°), and the proportion and density of forest cover (Dozier et al., 2008; Hall et al., 1998; Nolin, 2010). Forest cover is defined here as the fraction of the land surface obscured by tree canopy when viewed at nadir. Optical remote sensing is less accurate in forests as trees cast shadows (Kane et al., 2008; Vikhamar & Solberg, 2003), and the canopy conceals the surface where snow may exist (Liu et al., 2004, 2008). Except in cases of abrupt disturbances (e.g., fire, wind storms, beetle outbreak, or timber harvest), coniferous forests change over annual to decadal time scales, and thus the canopy is the most persistent obstacle to remote sensing of snow in forested, temperate areas. Forests are extensive, covering 40% of the North American snow zone (Klein et al., 1998), and as much as 50% of the Sierra Nevada snow zone (Richards, 1959). Quantifying MODIS errors in forests is critical for applications that rely on remotely sensed snow cover and snow disappearance timing (Raleigh & Lundquist, 2012).

* Corresponding author at: Box 352700, Seattle, WA 98195-2700, USA. Tel.: +1 206 685 7594; fax: +1 206 685 3836.
E-mail addresses: mraleig1@uw.edu (M.S. Raleigh), krittger@eri.ucsb.edu (K. Rittger), courtney_moore@fws.gov (C.E. Moore), bhenn@uw.edu (B. Henn), jlutz@uw.edu (J.A. Lutz), jdlund@uw.edu (J.D. Lundquist).

0034-4257/$ – see front matter © 2012 Elsevier Inc. All rights reserved.
http://dx.doi.org/10.1016/j.rse.2012.09.016

Canopy or vegetation adjustments are typically made to binary snow presence and fractional snow-covered area (f_{SCA}) MODIS products in forested areas. Klein et al. (1998) found that the normalized difference vegetation index (NDVI) improved mapping of MODIS binary snow cover with the normalized difference snow index (NDSI) in forested areas. For f_{SCA} retrievals, sub-canopy snow cover has been assumed equivalent to snow cover in the viewable gap (Liu et al., 2004), which adjusts (i.e., increases) the pixel f_{SCA} (Durand et al., 2008; Molotch & Margulis, 2008; Rittger et al., 2011). The accuracy of canopy adjustment methods for MODIS f_{SCA} is of prime interest, as viewable (i.e., canopy-free) f_{SCA} mapping with the physically-based MODIS Snow-Covered Area and Grain size algorithm (MODSCAG, Painter et al., 2009) has higher accuracy than NDSI-based empirical methods when using Landsat Enhanced Thematic Mapper Plus (ETM+) as validation (Rittger et al., 2012).

While prior studies have acknowledged the limitations of remote sensing of snow in forested regions (Hall et al., 1998, 2001, 2000; Klein et al., 1998; Liang et al., 2008; Liu et al., 2004; Nolin, 2010; Simic et al., 2004; Vikhamar & Solberg, 2003), a few studies have quantified the impact of increasing forest cover on MODIS snow mapping accuracy and the effectiveness of f_{SCA} canopy adjustments. Comparisons with Landsat TM in Alaska have indicated that the original MODIS binary snow mapping algorithm (Hall et al., 1995) has 96% accuracy in areas with <50% forest cover and 71% accuracy in areas with >50% forest cover (Hall et al., 1998). However, MODIS errors in forests cannot be reliably assessed with higher resolution sensors such as Landsat, because the Landsat sensor's line-of-sight is also obstructed by forest canopy and is susceptible to snow mapping errors from forest self-shadowing effects (Kane et al., 2008). Satellite intercomparison studies can yield uncertain conclusions because the highest resolution sensor is assumed to be the most accurate (Hall et al., 2000), even though all passive instruments have common limitations (e.g., forest canopy). Therefore, ground-based observations provide an independent and robust approach to validate MODIS and quantify snow cover mapping errors in forested areas.

Most MODIS ground-based validation studies have used daily snow observation networks (e.g., SNOTEL stations in the United States) that span regional and continental scales (Brubaker et al., 2005; Dong & Peters-Lidard, 2010; Klein & Barnett, 2003; Maurer et al., 2003; Parajka & Blöschl, 2008; Pu et al., 2007; Simic et al., 2004; Tekeli et al., 2005; Zhou et al., 2005). These networks provide insufficient information about the accuracy of MODIS or canopy adjustment methods in forested areas because measurement stations are typically located in clearings, which exhibit different snow accumulation and melt dynamics relative to forests (Varhola et al., 2010a). Additionally, the spatial density of observational networks is relatively sparse, with an average of 1 station per 100 km^2 in the most dense network (Parajka & Blöschl, 2008). MODIS pixels rarely encompass more than one ground-based snow sensor.

Intensive field surveys yield more dense spatial information to evaluate snow mapping in forests and the effectiveness of canopy correction methods. For example, the NASA Cold Land Processes Field Experiment (CLPX) (Cline et al., 2003) measured snow properties in subalpine forests and alpine areas in Colorado that have allowed evaluations of microwave remote sensing and examination of MODIS view angle effects in forests (Liu et al., 2008; Xin et al., 2012). CLPX teams sampled snow depth at 500 locations in nine 1 km^2 intensive study areas during 7 to 9 day periods near peak snow accumulation (late February and late March) in 2002 and 2003 (Elder et al., 2009). While the CLPX density (500 measurements per 1 km^2) is ideal, the timing of the observation periods (near peak accumulation) limits our understanding of potential snow cover mapping errors in the forest. The largest errors in remotely sensed snow cover are likely to occur late in the melt season when snow may persist longer in clearings (e.g., Storck et al., 2002) or in forests (e.g., Pomeroy & Granger, 1997). Field crews are rarely able to measure snow disappearance timing (Jost et al., 2007) because it requires frequent (e.g., daily) surveys through the melt season.

Shallowly-buried temperature sensors provide a robust, ground-based approach to monitor snow presence under the forest canopy and in clearings through an entire snow season (Lundquist & Lott, 2008). In temperate regions, diurnal fluctuations in near-surface soil temperatures are significantly reduced or absent when snow is present (Lundquist & Lott, 2008; Tyler et al., 2008), allowing inference of snow presence during damped temperature cycles at each sensor. By using a network of such sensors, f_{SCA} can be inferred and used to test MODIS-derived f_{SCA} and canopy adjustment methods in ways that higher spatial resolution imagery (e.g., Landsat) or typical ground-based monitoring stations (e.g., SNOTEL) cannot.

The purpose of this study is (1) to test the seasonal accuracy of f_{SCA} from canopy-adjusted MODSCAG through comparison with dense networks of daily ground-based observations at four sites in the California Sierra Nevada with varying forest cover, and (2) to validate the ground-based methodology. We validated our ground-based f_{SCA} during one snowmelt season at a meadow site using observations of daily snow depletion from time-lapse photography and high resolution (15 m) snow maps from the Advanced Spaceborne Thermal Emission and Reflection Radiometer (ASTER) (Yamaguchi et al., 1998).

2. Study sites and years

We selected four study sites (0.25 km^2 to 1.0 km^2) in the California Sierra Nevada (Fig. 1a, Table 1) across a range of forest cover. These included subalpine meadow sites at Tuolumne Meadows (TUM) and Dana Meadows (DAN), and forest sites at the Onion Creek Experimental Forest (ONN) and the Yosemite Forest Dynamics Plot (YFDP). All four sites have a Mediterranean climate, with the majority of annual precipitation falling between October and May, typically as snowfall (Baker, 1944; Serreze et al., 1999).

TUM and DAN are located in the headwaters of the Tuolumne River Basin in Yosemite National Park. TUM is located in a west-draining valley. A forested north-facing slope is found to the south, while a mixture of forest and rock outcroppings along a south-facing slope is found to the north. DAN is located 3 km west of Mt. Dana (3981 m) in a south-draining valley. Both meadow sites are flat, with mean slopes of 1° in TUM and 5° in DAN. Lodgepole pine (*Pinus contorta*) is the dominant tree species in these areas. Mean forest cover in the area surrounding each site is 23% at TUM and 32% at DAN (Table 1). The California Department of Water Resources (CDWR) measures SWE with snow pillows near each of these sites. SWE data were available at both sites through most of the study period, except after mid-February 2011 at TUM.

ONN is situated southwest of Donner Summit in the headwaters of the North Fork of the American River Basin. The study area spans 125 m of relief. Slopes are primarily southwest facing and measure 15° on average. The forest cover at ONN averages 65% and is primarily mixed-conifer forest, with communities of red fir (*Abies magnifica*), white fir (*Abies concolor*), Jeffrey pine (*Pinus jeffreyi*), and incense-cedar (*Calocedrus decurrens*), with discontinuous forest cover in montane chaparral and meadow. A prominent thicket of chaparral is found along the northwestern edge of the ONN study site, while a 0.2 km^2 dry meadow is located to the south. In this meadow, the National Oceanic and Atmospheric Administration (NOAA), through their Hydrometeorological Testbed (HMT, Ralph et al., 2005), maintains a meteorological station that monitors snow depth. This station provided reliable data until March 2011, when heavy snow accumulations buried and damaged the mast arms of the tower.

YFDP (http://www.yfdp.org) is located in the Tuolumne River Basin near Crane Flat in Yosemite National Park (Lutz et al., 2012). The site is predominantly north facing, with 18° mean slopes, and a 115 m elevation span. An old-growth forest comprised primarily of sugar pine

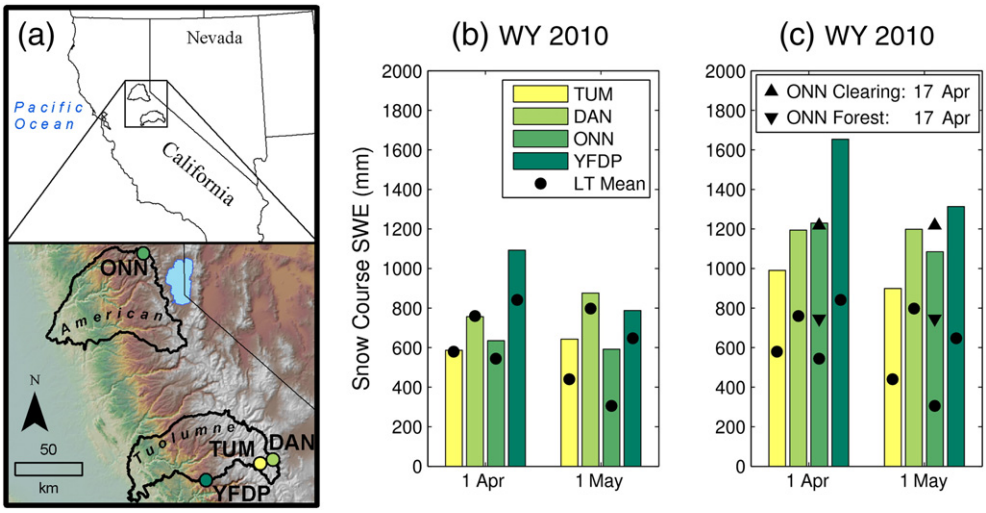

Fig. 1. (a) Locations of Tuolumne Meadows (TUM), Dana Meadows (DAN), Onion Creek Experimental Forest (ONN), and Yosemite Forest Dynamics Plot (YFDP) in the Sierra Nevada, and snow course snow water equivalent (SWE) at or near the four study sites during water years (b) 2010 and (c) 2011. Snow courses are from the California Cooperative Snow Survey network, taken routinely every year on or near 1 April and 1 May. YFDP is represented by the Gin Flat snow course, 4 km east of YFDP and 300 m higher in elevation. Also shown are the long-term (LT) means at each snow course on 1 April (n = 65 years) and 1 May SWE (n = 30 years); only years with snow at all four snow courses were used to calculate the LT mean. An additional snow survey on 17 April 2011 was conducted at ONN to document the difference in SWE accumulation between a clearing and the adjoining forest.

(*Pinus lambertiana*) and white fir (*A. concolor*) characterizes the site. Of the four study sites, YFDP has not only the highest mean forest cover (79%), but also the lowest mean elevation (1860 m).

The study spanned water years (i.e., 1 Oct–30 Sept) 2010 and 2011, which exhibited contrasting snow conditions according to monthly snow course measurements from the California Cooperative Snow Surveys (CCSS). During water year (WY) 2010, near average or above average snow conditions were found on 1 April, and above average conditions were found on 1 May due to additional snow storms and/or low melt rates throughout April (Fig. 1b). Water year 2011 featured anomalously high snow accumulations on both 1 April and 1 May (Fig. 1c). The CCSS surveys are made in clearings, where winter snow accumulations tend to be greater than under forest canopies. To measure the magnitude of this difference at ONN, we conducted a snow survey on 17 April 2011 at 47 points in the meadow and 51 points in the adjoining forest. Meadow SWE averaged 470 mm higher than forest SWE (Fig. 1c). The CCSS 1 April snow course measurements in ONN matched our 17 April meadow survey.

3. Methods

3.1. Ground-based f_{SCA}

In temperate snow zones such as the subalpine regions of the Sierra Nevada, diurnal fluctuations in sub-surface ground temperature (T_g) are damped or absent when snow is present because the low thermal conductivity of snow causes it to insulate the ground (Lundquist & Lott, 2008; Tyler et al., 2008). Thus, by measuring hourly T_g with shallowly-buried temperature sensors, daily snow presence can be inferred during periods with a reduced diurnal cycle in T_g (Fig. 2). Maxim (San Jose, California) Thermochron iButtons (model DS1922L) and Onset (Cape Cod, Massachusetts) HOBO Pendant data-loggers were deployed at TUM, DAN, and ONN to measure T_g every hour from August 2009 through July 2010, and from September 2010 through August 2011. Sensors measured hourly T_g at YFDP from November 2010 to July 2011. 92% of all sensors deployed in the study were iButtons, while the remaining 8% were HOBO Pendants. Sensors were buried 2 cm to 10 cm under the surface (Fig. 2a), following the methods of Lundquist and Lott (2008).

A network of temperature sensors sampled T_g across each study site at regular spatial intervals (Fig. 3). During WY 2010, paired sensors were located within 5 m to 10 m of each other, and all sets of paired sensors were located 100 m apart from each other on a quasi-regular grid (Fig. 3a, c, e). During WY 2011, the networks at TUM, DAN, and ONN were expanded to cover a larger area (Fig. 3b, d, f). Sensors were no longer paired at each location and were spaced every 100 m at TUM and ONN and every 100 m to 200 m at DAN. Sensors at YFDP (Fig. 3g) were only deployed in WY 2011, and were spaced every 40 m along two parallel transects. Sensors at TUM, DAN, and ONN were geolocated with a handheld GPS unit while sensors at YFDP were installed at study points that were surveyed with a total station.

Table 1
Characteristics of the four Sierra Nevada study sites, ordered by increasing forest cover.

	Tuolumne Meadows (TUM)	Dana Meadows (DAN)	Onion Creek (ONN)	Yosemite Forest Dynamics Plot (YFDP)
Mean forest cover[A], f_{can}	0.23	0.32	0.65	0.79
Latitude (N)	37° 52′ 30″	37° 53′ 58″	39° 16′ 40″	37° 45′ 59″
Longitude (W)	119° 21′ 49″	119° 15′ 20″	120° 21′ 18″	119° 49′ 9″
River basin	Tuolumne	Tuolumne	American	Tuolumne
Mean elevation (m)	2615	2985	1950	1860
Mean DJF air temperature[B] (°C)	−3.6	−4.1	−0.9	2.2
Mean annual precipitation[B] (mm)	830	970	1700	1060
WY 2010 ground sensors	45	45	89	–
WY 2011 ground sensors	47	52	75	37

[A] Average fractional forest cover of the 1500 m × 1500 m area encompassing each study site, based on the 30 m 2001 National Land Cover Dataset forest canopy product (Homer et al., 2004).
[B] Based on PRISM 1971–2000 monthly climate normals product at 800 m resolution (Daly et al., 2008, 1994).

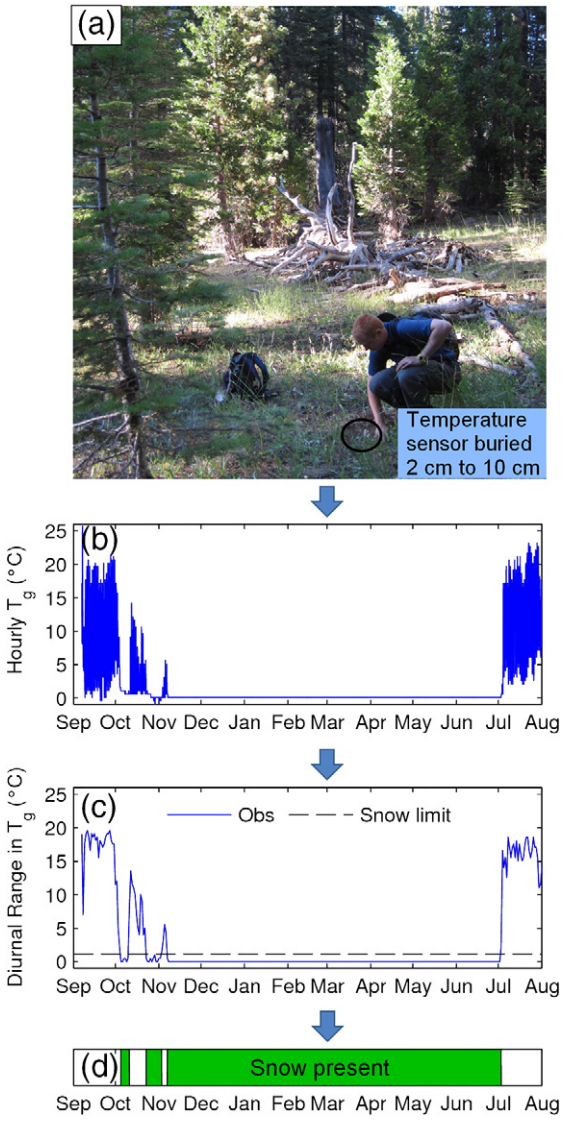

Fig. 2. Ground-based method of determining snow presence at a point with a self-logging temperature sensor. Temperature sensors were (a) buried at a depth of 2 cm to 10 cm and recorded (b) hourly ground temperature (T_g) through the study year. (c) Diurnal temperature ranges were inspected and periods with diurnal temperatures below 1.0 °C were (d) classified as snow-covered periods at that sensor.

After retrieving the sensors, all hourly T_g time series (Fig. 2b) were converted to daily time series of binary snow presence (i.e., 0 = snow-free, 1 = snow) with the following simple algorithm. To identify snow presence above a sensor, the algorithm required that the diurnal range in T_g did not exceed 1.0 °C over a period of 48 h (Fig. 2c). The resulting daily snow presence time series (Fig. 2d) were visually checked against the original hourly T_g. Additional quality control was conducted by comparing the timing of snowfall events (as observed at nearby snow pillows or as calculated based on air temperature and precipitation) to the snow time series at the study sites. This eliminated spurious snow detection during cold, snow-free periods in the autumn with low diurnal temperature variations. Averaged across the sites, spurious increases in f_{SCA} occurred on 10 days during WY 2010 and 3 days during WY 2011. When spurious snow presence was detected, we reclassified the affected sensors as snow-free.

To derive daily f_{SCA} time series at each site (hereafter called "ground f_{SCA}"), the number of sensors reporting snow presence each day was summed and divided by the total number of sensors at that site (Table 1). We checked the confidence of ground f_{SCA} through a Monte-Carlo type test at each site, where 10 sensors were randomly sampled to produce a unique f_{SCA} time series. This was repeated 100 times and the standard deviation of the 100 f_{SCA} time series was computed during each day of the ablation season. Averaged across the ablation season, the standard deviation of ground f_{SCA} ranged from 0.045 to 0.092, suggesting that the ground networks adequately sampled the snow cover dynamics of each study area.

3.2. Validation of ground f_{SCA}

To test ground f_{SCA}, we used two independent observations of snow cover depletion at TUM during the spring and summer of 2010. These included a time-lapse camera, which was used to check the timing and rate of snow cover depletion, and three high-resolution (15 m) images from ASTER in a canopy-free area, which were used to further assess f_{SCA} accuracy.

3.2.1. Time-lapse analysis

An east-facing time-lapse camera took a photograph of Tuolumne Meadows every four hours in May and June 2010 and recorded the depletion of snowpack from full cover to snow-free conditions. The camera was located approximately 2 km west of the TUM ground sensors and focused on the western area of the meadow, which we assumed had similar snow depletion timing and rates to the meadow as a whole. The camera, a Sony Cybershot (model DSC-W55) with 7.2 megapixel resolution, was placed in a protective casing and fixed to a tree for stability.

Numerous studies have employed time-lapse photography to assess patterns of snow presence, to quantify spatial and temporal components of snow cover depletion at small scales, and to measure snow depth (see Parajka et al., 2012 for a review). We employed a novel approach for detecting the temporal depletion of snow by mapping snow cover in each scene based on pixel brightness and then using singular value decomposition (SVD) (see Wall et al., 2003) to extract the temporal depletion information. SVD is the basis for Principal Component Analysis (PCA), which is essentially equivalent to Empirical Orthogonal Function (EOF) analysis. SVD reduces a complex system into its principal modes of variability; in other words, it finds the signals that explain the most variance of the data set in space and time.

Daily images (e.g., Fig. 4a–c) taken between 10 AM and 2 PM PST were retained to coincide with the overpass of Terra (10:30 AM equatorial crossing), to minimize shadows in the image, and to ensure relatively consistent lighting from day-to-day. Cloudy images were removed because they introduced noise in the analysis by reducing the lighting in each scene. We converted each image from RGB to the 0 to 255 range (0 = black and 255 = white) in order to map snow cover based on grayscale brightness. We confined the analysis to an area in the western extent of the meadow (i.e., closer to the camera) to reduce distortion of pixels, as pixels farther from the camera encompassed more land surface area than pixels closer to the camera.

A snow mapping algorithm was used and demonstrated to be consistent with visually identified snow cover in each original RGB image. To map snow in each grayscale image, we constructed a histogram and classified snow-covered pixels by finding pixel brightness values greater than 155 (~60% brightness), which corresponds to the lower limit of snow albedo at visible wavelengths for shallow snow with a large grain radius (Wiscombe & Warren, 1980). The algorithm translated each grayscale image into a binary snow map. The binary snow map of each image was reordered into a column vector, and a matrix (**M**) was constructed from all vectors, such that rows corresponded to spatial position and columns corresponded to time.

SVD was then used to derive the temporal component of snow depletion. **M** was input into the SVD.m routine in MATLAB (Version 7.9), which output the spatial and temporal modes, ordered by the proportion of variance explained. The first mode explained 34% of the variance in the time-lapse sequence, and the non-zero spatial weights indicated that this mode represented snow cover (Fig. 4d).

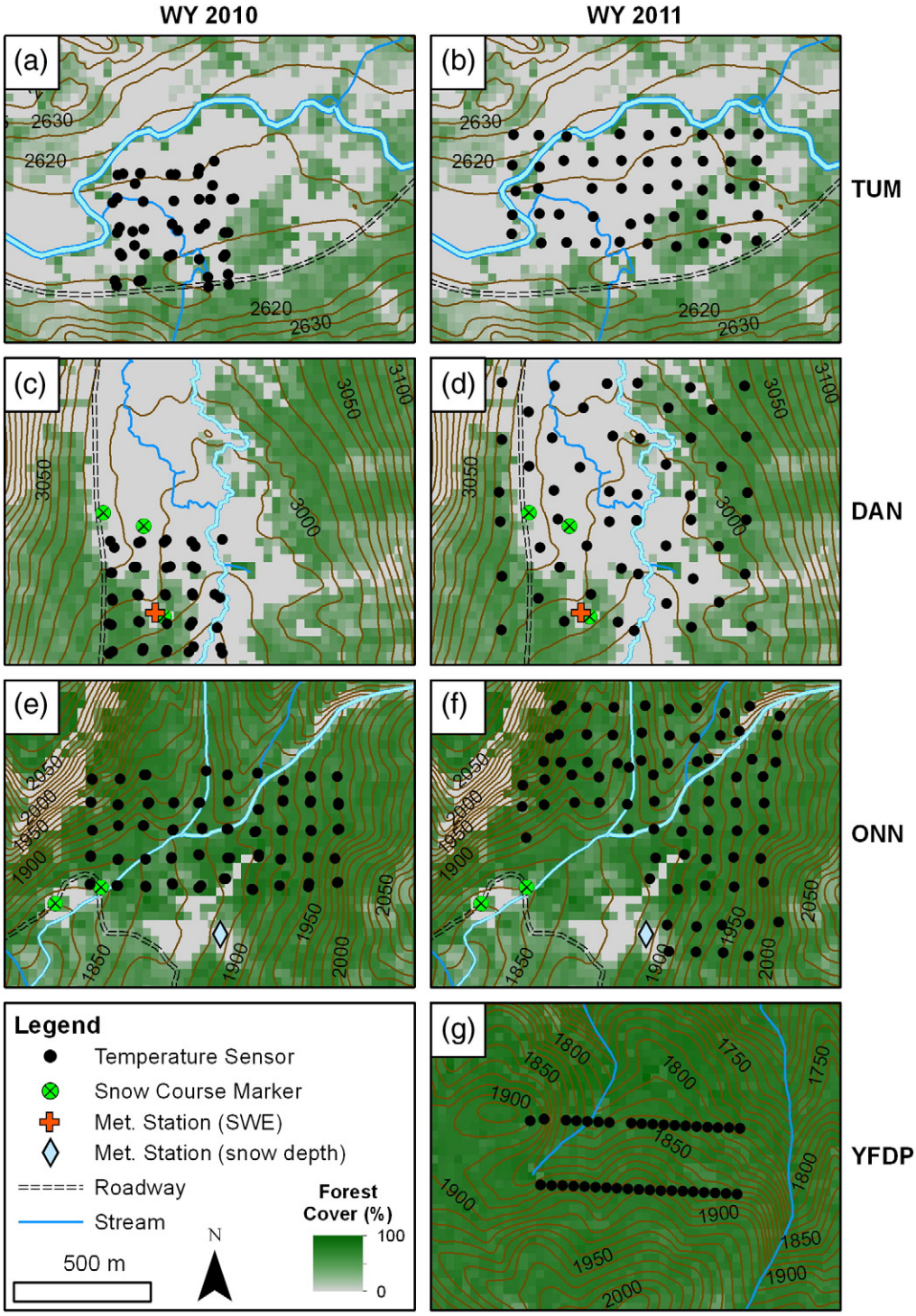

Fig. 3. Locations of ground temperature sensors at the study sites during water years 2010 and 2011. Shown in order of increasing forest cover are (a–b) Tuolumne Meadows, (c–d) Dana Meadows, (e–f) Onion Creek, and (g) the Yosemite Forest Dynamics Plot. Most locations during WY 2010 (a, c, e) have two temperature sensors in close proximity (<10 m) but appear as a single dot. Contour interval is 5 m in (a) and (b), and 10 m in all other subplots.

Thus, the first temporal mode (Fig. 4e) described how snow cover depleted through time. To infer a time series of f_{SCA}, the absolute value of the first temporal mode was scaled to the 0 to 1 range, hereafter called "time-lapse f_{SCA}" (Fig. 4e).

3.2.2. ASTER

Cloud-free ASTER images of TUM were obtained on 25 April, 5 June, and 30 July in 2010 to derive high resolution snow maps. ASTER visible and near infrared (VNIR) bands in the green–yellow (0.520–0.600 μm), red (0.630–0.690 μm), and near-infrared (0.780–0.860 μm) wavelengths were acquired. Supervised mapping of snow cover was implemented based on the methods of Vogel (2002), which were developed for the 15 m panchromatic band (0.52–0.92 μm) of Landsat 7 and found to have comparable performance to the NDSI approach. The raw digital numbers of each ASTER channel were first converted to radiance and reflectance based on NASA

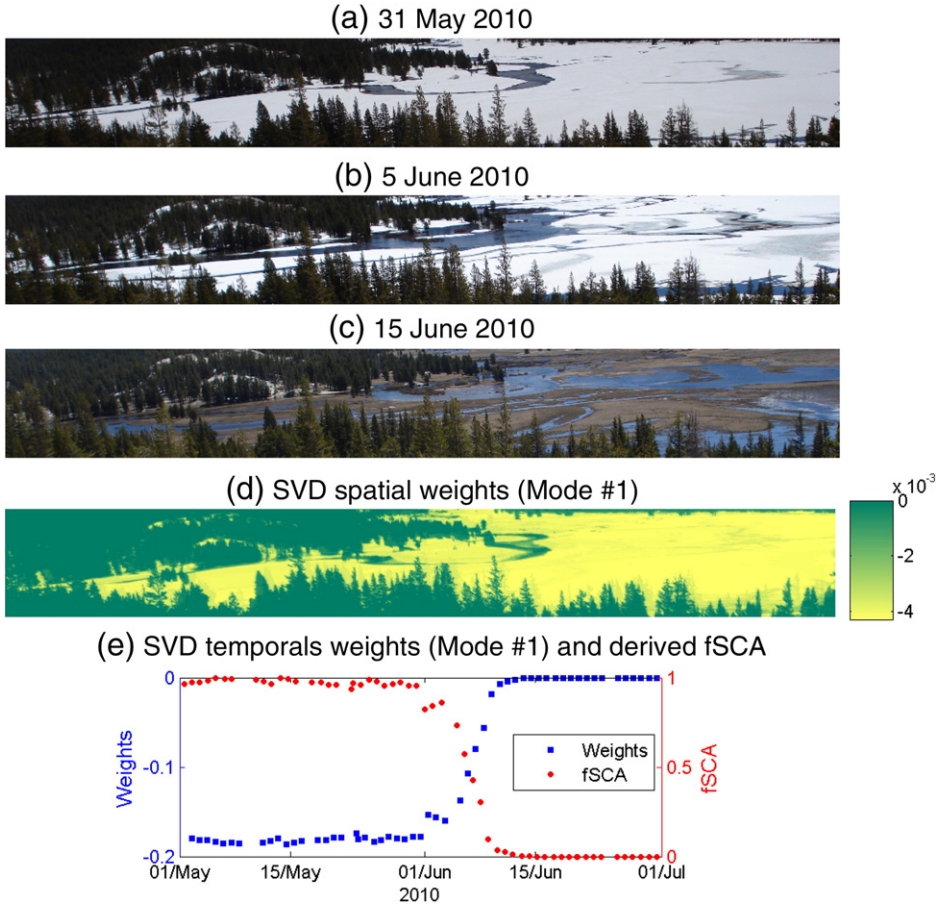

Fig. 4. Tuolumne Meadows time-lapse photo analysis with singular value decomposition (SVD) during May–June 2010. Shown are sample RGB photographs taken to show progression of snow cover from (a) 31 May to (b) 5 June to (c) 15 June. Also shown are the (d) spatial and (e) temporal weights of the 1st SVD mode, which is interpreted as snow cover depletion. A fractional snow-covered area (f_{SCA}) time series was inferred from the temporal weights of the 1st SVD mode.

(2001). The VNIR reflectance values in each pixel were then averaged into a single panchromatic value. Pixels with panchromatic reflectance > 40% were mapped as snow, consistent with the NDSI threshold (Dozier, 1984). This threshold provided the best visual match to false-color images of snow cover (Fig. 5). ASTER f_{SCA} was acquired in a 465 m square box coincident with the study area, and sized to exclude adjoining forested areas.

The number of snow-covered ASTER pixels divided by the total number of ASTER pixels (961) in the area (red box, Fig. 5b) was taken as ASTER f_{SCA}. We carefully considered the accuracy of this approach, as fine resolution maps of binary snow cover may have bias when aggregated to a coarse f_{SCA} value (Rittger et al., 2012). As noted by Rittger et al. (2012), binary methods may underestimate snow cover at low fractions and overestimate snow cover at higher fractions. However, we did not find evidence that a major bias in ASTER f_{SCA} existed at TUM in 2010.

3.3. MODIS Snow-Covered Area and Grain Size (MODSCAG)

The physically-based MODSCAG algorithm uses spectral mixture analysis on a pixel-by-pixel basis to derive gridded 500 m daily f_{SCA}. Spectral mixture analysis finds the best linear combination of land surface endmembers (e.g., snow, soil, rock, vegetation, lake ice) that matches MODIS surface reflectance from the Terra MOD09GA product (Painter et al., 2009):

$$R_{S,\lambda} = \sum_i f_i R_{\lambda,i} + \varepsilon_\lambda \quad (1)$$

where $R_{S,\lambda}$ is the pixel-averaged surface reflectance from MOD09GA at wavelength λ, f_i is the fraction of endmember i in the pixel, $R_{\lambda,i}$ is the surface reflectance for endmember i at wavelength λ, and ε_λ is the residual error for all endmembers. Wavelength-dependent surface reflectance of non-snow endmembers (e.g., vegetation, soil) is acquired from a library of observations acquired in the field or in a laboratory. Snow reflectance is estimated using a hemispherical directional reflectance factor and a discrete-ordinates radiative transfer model. Using the approach in Eq. (1), MODSCAG examines permutations of two or more endmembers and selects the model with the smallest error (relative to MOD09GA reflectance) and the fewest endmembers. If this combination of endmembers includes snow, then the daily f_{SCA} is computed as the fraction of the snow endmember, normalized by the fraction of photometric shade (e.g., due to terrain or vegetation shading) in the pixel. The lower detection limit is $f_{SCA} = 0.15$ (Painter et al., 2009). For a complete description of the MODSCAG algorithm, the interested reader is directed to the model development paper of Painter et al. (2009). MODSCAG snow cover data are available through the NASA JPL Snow Data System Portal (http://snow.jpl.nasa.gov/).

After implementation of MODSCAG at all pixels and all daily scenes, cloudy and noisy pixels are filtered, producing gaps. Noisy pixels usually occur when one or more spectral bands have high frequency dropouts to zero reflectance, which cannot be used to estimate the snow cover properties of a pixel (Dozier et al., 2008). Therefore, noisy pixels require removal and estimation through interpolation. MODSCAG scenes were interpolated in time using a 16-day smoothing spline on a pixel-by-pixel basis following Dozier et al.

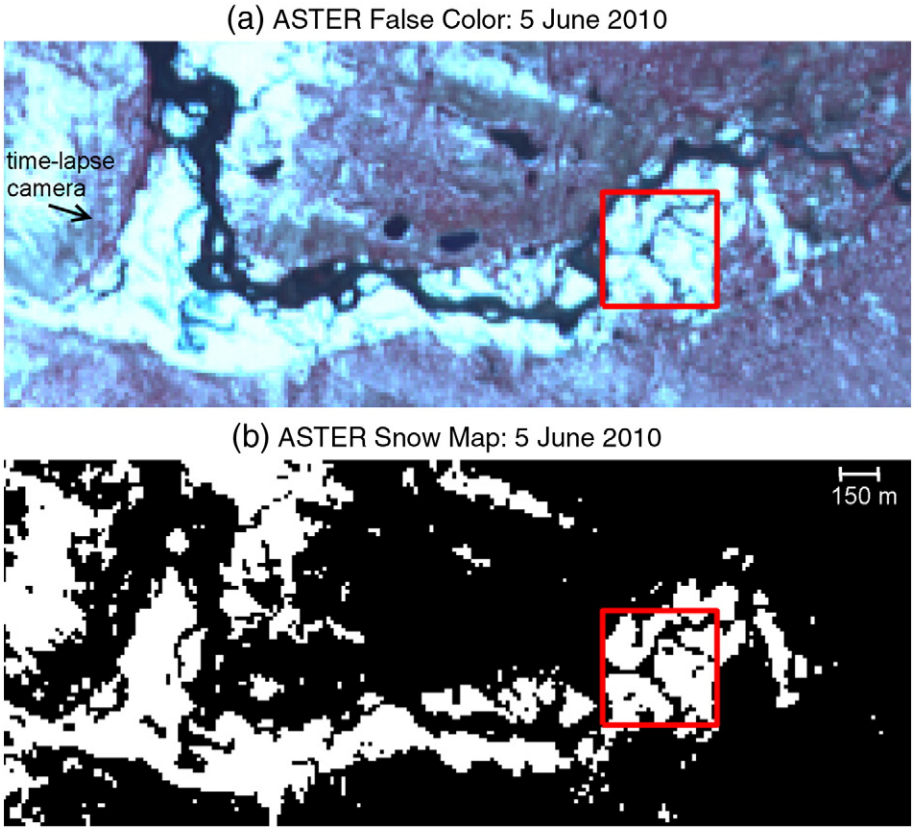

Fig. 5. (a) ASTER nadir false color image (RGB 321) of Tuolumne Meadows on 5 June 2010, showing snow cover and melt water channels draining to the Tuolumne River. The approximate location and view direction of the time-lapse camera (Fig. 4) are indicated. ASTER VNIR resolution is 15 m. (b) Mapped snow cover from the ASTER image on 5 June 2010 (white = snow cover, black = snow-free or unknown). The red box corresponds to the approximate location of the ground temperature sensors from Fig. 3a. Fractional snow cover in the red box was 0.66 on this date.

(2008) and Dozier and Frew (2009). The implemented spline (csaps.m in MATLAB) was a weighted combination of a least-squares fit and a cubic spline. The best fit changed depending on the temporal spacing between available data, and therefore varied spatially as a result of non-uniformities in cloud cover and noisy data. Estimates from the spline were additionally weighted according to the cosine of the sensor view zenith angle and the view-angle-dependent pixel area, such that near-nadir views had the greatest weights.

Filtering and smoothing of the MODSCAG scenes produced a temporally continuous product of gridded daily f_{SCA} across the Sierra Nevada. Because the geolocation accuracy of MODIS (± 1.5 pixels) and the gridding procedure may introduce artifacts into a pixel-scale validation (Tan et al., 2006), we aggregated (i.e., averaged) the MODSCAG f_{SCA} in a 3×3 (i.e., 1500 m $\times$ 1500 m) pixel window encompassing each site to ensure collocation with the area sampled by the ground-based observations (Xin et al., 2012).

3.4. MODSCAG canopy adjustments

MODSCAG f_{SCA} is created based on the land surface that is viewable by MODIS, which underestimates snow cover in forests due to effects such as canopy obstruction (Rittger et al., 2012). In forested areas, only the land surface in forest clearings, canopy gaps, and between canopy gaps is visible (Liu et al., 2008). These viewable areas provide the basis for estimating f_{SCA} with MODSCAG, which currently lacks a native canopy adjustment. We adjusted the MODSCAG f_{SCA} time series by the viewable gap fraction (VGF), which can be provided by a geometric optical model (Liu et al., 2004) or a satellite-derived product (Durand et al., 2008; Molotch & Margulis, 2008; Rittger et al., 2012):

$$f_{SCA,adjusted} = \frac{f_{SCA,obs}}{1 - f_{can}} \tag{2}$$

where $f_{SCA,adjusted}$ is the MODSCAG f_{SCA} adjusted for forest canopy, $f_{SCA,obs}$ is the f_{SCA} from the gridded daily 500 m MODSCAG product, $1 - f_{can}$ is the viewable gap fraction, and f_{can} is the fractional forest cover of each grid cell. This adjustment increases f_{SCA} in areas with trees to account for the area hidden by the canopy and the greatest f_{SCA} adjustments occur in more dense forests. $f_{SCA,adjusted}$ is constrained to the [0, 1] interval. This canopy-adjusted MODSCAG f_{SCA} is hereafter referred to as "MODSCAG f_{SCA}".

For the value of f_{can} (Eq. 2) at each site, we used the static (i.e., temporally constant) percent tree canopy from the 2001 National Land Cover Dataset (NLCD), which is derived from Landsat 5 and Landsat 7 data at 30 m resolution (Homer et al., 2004; USGS, 2011). This dataset is freely available and commonly used in snow research (e.g., Durand et al., 2008; Young et al., 2009). Changes in land cover at the sites were insignificant between 2001 and 2011.

There are several well-known limitations inherent in this canopy adjustment (Rittger et al., 2012). First, this correction assumes f_{SCA} under the forest canopy is equivalent to f_{SCA} in the viewable areas (e.g., meadows, clearings) (Durand et al., 2008). However, snow studies across different climate zones show accumulation and melt rates change based on forest cover and type of tree (see Varhola et al., 2010a). Viewable snow in a clearing is not likely to represent snow

under the canopy, especially late in the melt season. Second, the simplifying assumption of constant f_{can} for MODIS may not be robust in areas with trees, as a greater area of each tree (e.g., leaves, branches, trunks) will be included as the view angle increases (Hall et al., 1998; Liu et al., 2008). While the smoothing algorithm weights $f_{SCA,obs}$ based on view angle and pixel area (see Section 3.3), a weighting scheme is ineffective for static values of f_{can}, and therefore the static approach may not be fully sufficient. Third, a static adjustment is not robust when forest canopies are loaded with snow, as immediately following a precipitation event.

3.5. Evaluation metrics

We adopted the same binary and fractional metrics for evaluation as prior MODSCAG studies (Painter et al., 2009; Rittger et al., 2012) and other MODIS snow cover studies (e.g., Dong & Peters-Lidard, 2010). The binary metrics are first-order performance metrics that reveal the accuracy of MODSCAG in determining whether or not snow is present, regardless of the fractional value. Fractional metrics are used to assess actual f_{SCA} errors. MODSCAG f_{SCA} values below the MODSCAG detection limit (0.15) were set to 0 before calculating the binary and fractional metrics. Ground f_{SCA} values below 0.15 were not changed in this manner, as this indicated the existence of patchy snow.

3.5.1. Binary metrics

During each day of the snow season at each study site, MODSCAG f_{SCA} was evaluated based on the agreement or disagreement of snow presence with the ground f_{SCA}. Days when snow was present (i.e., $f_{SCA} \geq 0.15$ for MODSCAG, $f_{SCA} \geq 0$ for ground) in both ground f_{SCA} and MODSCAG f_{SCA} were classified as a true positive (TP), while days when both reported snow-free conditions (i.e., $f_{SCA} < 0.15$ for MODSCAG, $f_{SCA} = 0$ for ground) were classified as a true negative (TN). A false positive (FP) indicated that MODSCAG identified snow cover not observed by the ground network (i.e., commission), and a false negative (FN) signified that MODSCAG missed snow cover that the ground network observed (i.e., omission). These daily values were input into three binary metrics to determine performance across the snow season:

$$Precision = \frac{TP}{TP + FP} \tag{3}$$

$$Recall = \frac{TP}{TP + FN} \tag{4}$$

$$F = \frac{2TP}{2TP + FP + FN}. \tag{5}$$

Precision tests for commission errors, *Recall* tests for omission errors, and the *F* score tests for both errors. All three binary metrics vary from 0 to 1, with 1 indicating perfect performance.

3.5.2. Fractional metrics

Direct comparisons of MODSCAG f_{SCA} and ground f_{SCA} were achieved through the use of mean bias (i.e., mean difference), median bias, and root mean squared error (RMSE):

$$RMSE = \sqrt{\frac{1}{N}\sum_{N}\left(fSCA_{MODSCAG} - fSCA_{ground}\right)^2} \tag{6}$$

where N is the number of snow-covered days, as observed at each ground network. Bias was taken as the difference between MODSCAG f_{SCA} and ground f_{SCA}, such that a positive (negative) bias indicated MODSCAG overestimated (underestimated) f_{SCA}.

4. Results

4.1. Validation of ground f_{SCA} at Tuolumne Meadows

Comparisons of ground f_{SCA} against time-lapse f_{SCA} and ASTER f_{SCA} in 2010 indicated that the ground f_{SCA} methodology was accurate. Time-lapse f_{SCA} and ground f_{SCA} matched each other in characterizing the timing and rate of snow cover depletion from late May to early June 2010 (Fig. 6a). Both ground f_{SCA} and time-lapse f_{SCA} indicated that the majority of snow cover depletion occurred over a ten day period (29 May to 8 June). During this critical melt period, ground f_{SCA} had high correlation ($R^2 = 0.98$) with time-lapse f_{SCA}.

Ground f_{SCA} tracked ASTER f_{SCA} across the three available ASTER images (Fig. 6a). Ground f_{SCA} on 25 April 2010 (full snow cover) and 30 July 2010 (no snow cover) matched ASTER f_{SCA}. A comparison on 5 June 2010 supported the accuracy of ground f_{SCA} during the critical melt out period, as ground f_{SCA} was 0.62 and ASTER f_{SCA} was 0.66 (Fig. 5b). ASTER was valuable in that it provided additional f_{SCA} information in early June 2010, when MODSCAG snow cover disappeared abruptly (see Section 4.2.1).

4.2. Time series comparisons

4.2.1. Tuolumne Meadows (TUM)

Across the 2010 and 2011 snow seasons, MODSCAG had high *Precision* and *F* score values at TUM (Table 2). MODSCAG performance was better in 2011 than 2010 because omission errors (*Recall*) were present during the 2010 melt season, likely from cloud cover and view angle issues (described below). Omission errors also arose when MODSCAG either missed early season storms or the smoothing algorithm removed snow storms in October 2010 and 2011 (Fig. 6).

The canopy adjustment reduced MODSCAG f_{SCA} bias at TUM by 13% to 15% during the two years (Fig. 6), but canopy-adjusted MODSCAG still had a consistent negative bias at TUM during both years (Table 3). During the winter months, MODSCAG f_{SCA} oscillated between 0.60 and 0.95 in a pattern possibly introduced by the smoothing method (Section 3.3); these multi-day f_{SCA} oscillations during the winter were a common feature of MODSCAG f_{SCA} at all four sites. At TUM, these oscillations did not consistently coincide with snowfall events, and therefore did not occur due to increased reflection from canopy interception.

A notable MODSCAG f_{SCA} error at TUM occurred in spring 2010 when MODSCAG f_{SCA} depleted rapidly and fell below the 0.15 threshold on 1 June, 7 days before the ground f_{SCA} and 8 days before the time-lapse f_{SCA} fell below 0.15 (Fig. 6a). An examination of atmospheric transmissivity (calculated from insolation observations) and MODIS visible imagery indicated that cloudy conditions persisted on 1 June, 3 June, and 4 June (Fig. 7a). Additionally, the Terra satellite was off-nadir (i.e., >30°) on 31 May (31°), 2 June (43°) and 6 June (49°). The limited availability of near-nadir view angles on clear days within the short snow cover depletion period (29 May–8 June) likely caused MODSCAG f_{SCA} to decline rapidly on 1 June. Interestingly, SWE at the TUM snow pillow disappeared on 3 June 2010, two days after MODSCAG f_{SCA} fell below 0.15 (Fig. 6a).

4.2.2. Dana Meadows (DAN)

MODSCAG had the fewest omission errors at DAN, as noted by the high *Recall* values. MODSCAG *Precision* (Table 2) was also high at DAN, and the main commission errors occurred in early October 2009 and 2010, and briefly in mid-October 2010 (Fig. 8).

The canopy adjustment reduced MODSCAG f_{SCA} bias by 22% to 23% during the two years (Fig. 8), but canopy-adjusted MODSCAG f_{SCA} still had an overall negative bias at DAN (Table 3). In both years, MODSCAG overestimated f_{SCA} during the early accumulation season (e.g., October) but underestimated f_{SCA} through the period of full snow cover (e.g., December through early June), with values typically

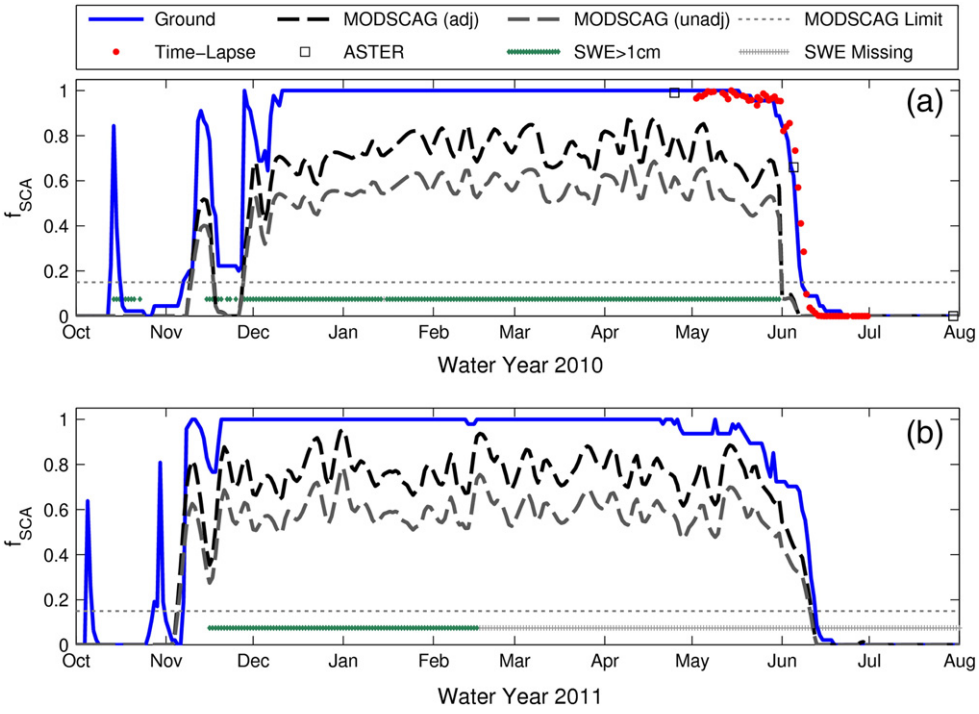

Fig. 6. Fractional snow-covered area (f_{SCA}) at Tuolumne Meadows (TUM) during water years (a) 2010 and (b) 2011. Shown in both years are f_{SCA} from the ground temperature network, and MODSCAG f_{SCA} before and after the canopy adjustment. In May–June 2010, independent f_{SCA} data from a time-lapse camera and ASTER were included for validation. Also shown are periods when the TUM snow pillow reported snow presence (SWE > 1 cm) and when SWE data were missing.

fluctuating between 0.75 and 0.96. During the 2010 ablation season, MODSCAG f_{SCA} reasonably matched ground f_{SCA} (Fig. 8a). During the 2011 ablation season, MODSCAG had a notable f_{SCA} overestimation error from 28 June to 30 June (Figs. 7b, 8b), possibly introduced by cloud cover and off-nadir view angles. After this period, MODSCAG f_{SCA} reasonably tracked the ground f_{SCA} for the rest of the 2011 ablation season. Complete depletion of MODSCAG f_{SCA} (i.e., $f_{SCA}<0.15$) was only 1 to 2 days earlier than ground f_{SCA} depletion during the two years. During 2010, snow disappeared at the DAN snow pillow on 24 June, which was 1 day prior to MODSCAG and 2 days prior to the ground temperature network. In 2011, snow disappeared at the DAN snow pillow on 1 July, 7 days prior to MODSCAG and 9 days prior to the ground network.

4.2.3. Onion Creek Experimental Forest (ONN)

MODSCAG yielded more omission errors at ONN than at DAN, as suggested by lower *Recall* (Table 2). Omission errors occurred in November 2009, October 2010, and during the second half of the melt season in both water years (Fig. 9). The high *Precision* indicated that commission errors were rare at ONN, which increased the *F* score.

The canopy adjustment had the greatest bias reduction at ONN, with bias reduced by 35% to 42% during the two years (Fig. 9). However, canopy-adjusted MODSCAG f_{SCA} had a negative bias through both years at ONN (Table 3). The largest f_{SCA} errors occurred during the early accumulation and late ablation seasons (Fig. 9). During the 2010 ablation season, MODSCAG f_{SCA} abruptly depleted and dropped below the 0.15 detection threshold on 1 June 2010 (Fig. 9a). This date of complete snow depletion at ONN was 2 days prior to the date of snow disappearance at the NOAA HMT snow depth sensor, but 11 days prior to the ground temperature sensors. MODSCAG f_{SCA} depletion was more gradual during the 2011 ablation season (Fig. 9b), but reported systematically lower f_{SCA} through this period and reached complete depletion 12 days prior to the ground sensors. During both ablation seasons, MODSCAG snow cover disappeared (i.e., $f_{SCA}<0.15$) once ground f_{SCA} approached the forest cover fraction (Fig. 7c).

4.2.4. Yosemite Forest Dynamics Plot (YFDP)

MODSCAG had the lowest *Recall* and *F* score at the heavily forested YFDP (Table 2), indicating that snow omission errors were most common at this site. Omission errors were concentrated in May 2011 when the snow cover was melting (Fig. 10). Sporadic periods with MODSCAG omission errors were also present during periods of partial snow cover disappearance in the middle of the snow season (e.g., early December, early February). Like ONN, commission errors were rare at the YFDP, as *Precision* was high.

Table 2
Summary of binary metrics across each snow season at the four study sites.

Metric	Water year	TUM	DAN	ONN	YFDP
Precision	2010	1.00	0.96	1.00	–
	2011	0.99	0.97	0.99	0.96
	Mean	1.00	0.96	1.00	0.96
Recall	2010	0.78	0.94	0.80	–
	2011	0.91	0.98	0.88	0.61
	Mean	0.84	0.96	0.84	0.61
F score	2010	0.87	0.95	0.89	–
	2011	0.95	0.97	0.93	0.75
	Mean	0.91	0.96	0.91	0.75

Table 3
Summary of fractional metrics across each snow season at the four study sites.

Metric	Water year	TUM	DAN	ONN	YFDP
RMSE	2010	0.28	0.19	0.24	–
	2011	0.23	0.19	0.17	0.55
	Mean	0.25	0.19	0.21	0.55
Mean bias	2010	−0.24	−0.11	−0.11	–
	2011	−0.19	−0.08	−0.07	−0.37
	Mean	−0.22	−0.09	−0.09	−0.37
Median bias	2010	−0.25	−0.15	−0.03	–
	2011	−0.20	−0.12	−0.03	−0.41

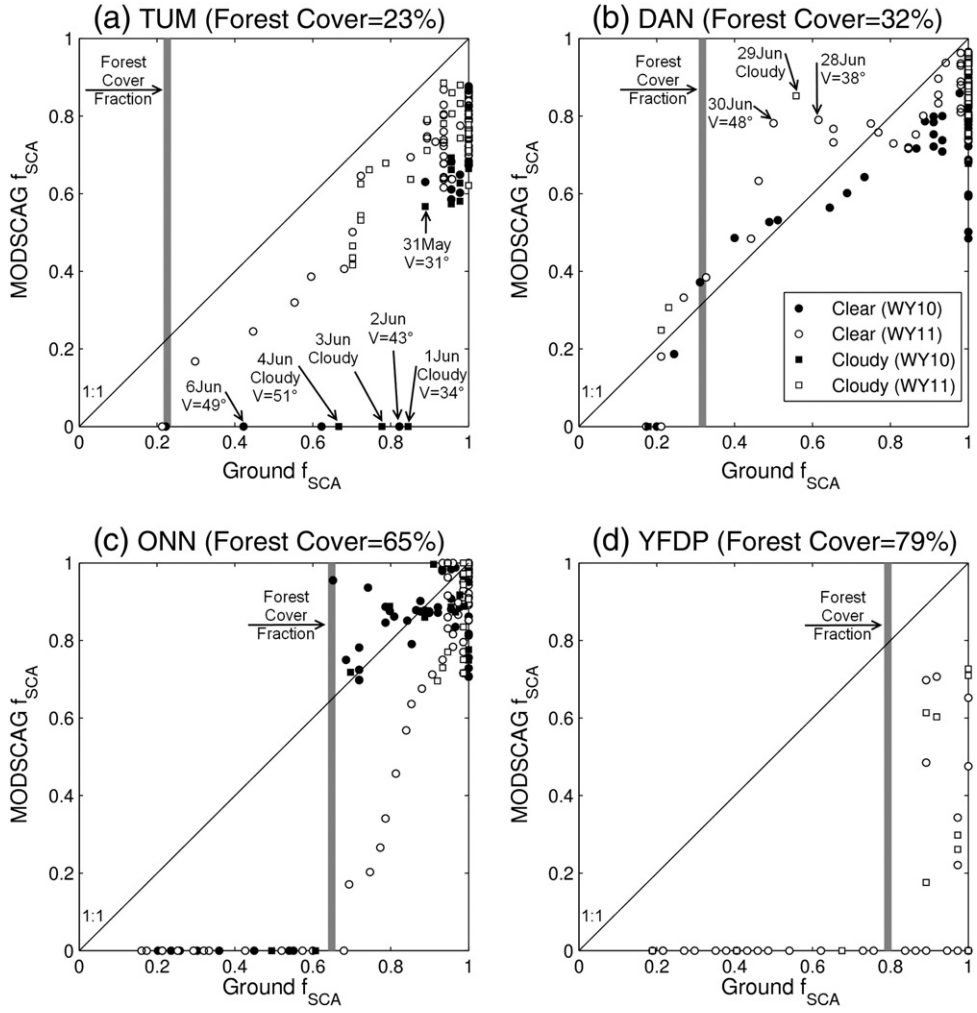

Fig. 7. Ground fractional snow-covered area (f_{SCA}) vs. canopy-adjusted MODSCAG f_{SCA} at (a) Tuolumne Meadows, (b) Dana Meadows, (c) Onion Creek, and (d) the Yosemite Forest Dynamics Plot from 1 April to melt out during water years 2010 and 2011. Time generally progresses from the upper right corner to the lower left as the snow cover disappears. Points are classified based on whether cloudy or clear conditions prevailed, based on pyranometer data and MODIS visible imagery. Points during a one week period in WY 2010 at TUM (a) and during a three day period in WY 2011 at DAN (b) are labeled to indicate a combination of cloudy days and off-nadir view angles (V) that introduced errors in MODSCAG f_{SCA}. The NLCD forest cover fraction is also plotted, showing that MODSCAG f_{SCA} drops to 0 at the forest sites (c, d) as the ground f_{SCA} approaches the forest fraction.

While *Precision* was high at YFDP, errors in f_{SCA} were prevalent throughout the 2011 snow season (Fig. 10), as MODSCAG f_{SCA} had a RMSE of 0.55 and a mean bias of −0.37 (Table 3). In other words, MODSCAG reported that snow cover existed throughout most of the snow season, but MODSCAG f_{SCA} was generally too low. MODSCAG f_{SCA} was characterized by multiple cases with rapid increases to full snow cover and nearly equivalent drops in f_{SCA} within 1 to 2 weeks. These large fluctuations were not found in the ground f_{SCA} (Fig. 10).

Comparing the MODSCAG f_{SCA} time series to snow accumulation data at the nearby Gin Flat snow pillow indicated that the MODSCAG f_{SCA} fluctuations often coincided with new snowfall events (Fig. 10). This suggested either MODSCAG was viewing intercepted snow in the forest canopy, or storm clouds were being misclassified as snow cover, or some combination thereof due to the smoothing algorithm. However, not all f_{SCA} fluctuations coincided with new snow events at YFDP (e.g., single peak in early November, two peaks in mid-April).

During the 2011 ablation season, MODSCAG only mapped snow cover at YFDP when the ground f_{SCA} was greater than the forest cover fraction (Fig. 7d), as at ONN. A snowfall event in mid-May 2011 brought ground f_{SCA} back to full cover and extended the snow season by 9 days. MODSCAG missed this snowfall event, as it reached complete depletion ($f_{SCA}<0.15$) prior to this storm (26 April) and remained below the 0.15 threshold through the summer. Ground f_{SCA} reached 0.15 on 26 May, 30 days after MODSCAG (Fig. 10).

4.3. Seasonality of errors

We found that MODSCAG errors varied relative to forest cover and time of year. We examined how errors changed across three periods: the early accumulation season (first day of $f_{SCA}\geq0.15$ through 31 December), the winter (1 January through 31 March), and the ablation season (1 April to the final day of $f_{SCA}\geq0.15$). At TUM, DAN, and ONN, MODSCAG errors tended to be the most variable during the accumulation and ablation seasons (Fig. 11a, c). Errors at these three sites were generally less variable during the winter months (Fig. 11b). At YFDP, MODSCAG tended to underestimate snow cover more severely and more consistently with time (Figs. 10, 11).

5. Discussion and conclusions

We demonstrated that networks of temperature sensors buried shallowly in the ground provide reliable values of daily f_{SCA}, which can be used to test canopy-adjusted MODSCAG f_{SCA} in forest locations not sampled by traditional methods (e.g. Landsat, SNOTEL sites). At

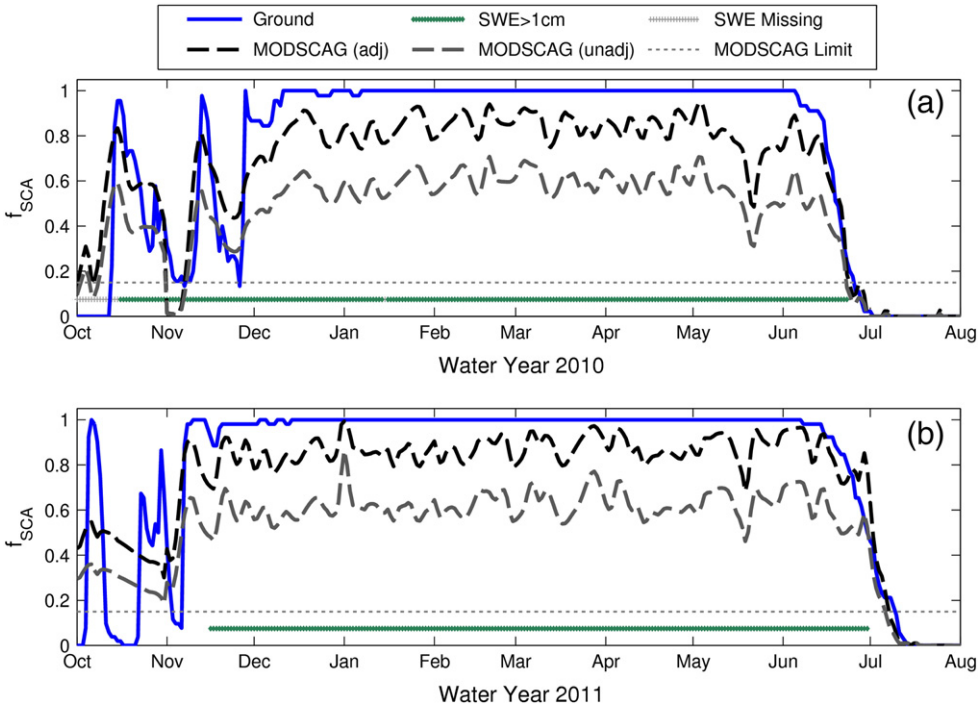

Fig. 8. Fractional snow-covered area (f_{SCA}) at Dana Meadows (DAN) from the ground temperature network and MODSCAG during water years (a) 2010 and (b) 2011. MODSCAG f_{SCA} is shown before and after the canopy adjustment. Also shown are periods when the DAN snow pillow reported snow presence (SWE > 1 cm) and when SWE data were missing.

our Sierra Nevada sites, we found that (1) the static canopy adjustment (Eq. 2) reduced MODSCAG f_{SCA} bias (Figs. 6, 8–10) but a consistent negative bias still remained (Fig. 11 and Table 3), (2) the accuracy of canopy-adjusted MODSCAG f_{SCA} varied with forest cover, and (3) MODSCAG errors were usually most variable during the accumulation and ablation seasons. The results demonstrated the value of dense ground-based validations of remote sensing and underscored the need for improved canopy adjustments for MODIS f_{SCA}.

Canopy-adjusted MODSCAG f_{SCA} was systematically lower than ground f_{SCA} during the middle of winter (Fig. 11b). This result was particularly surprising at the meadow sites (TUM and DAN), as we expected full snow cover at these flat, lightly forested, high-elevation locations, which had considerable snow accumulation

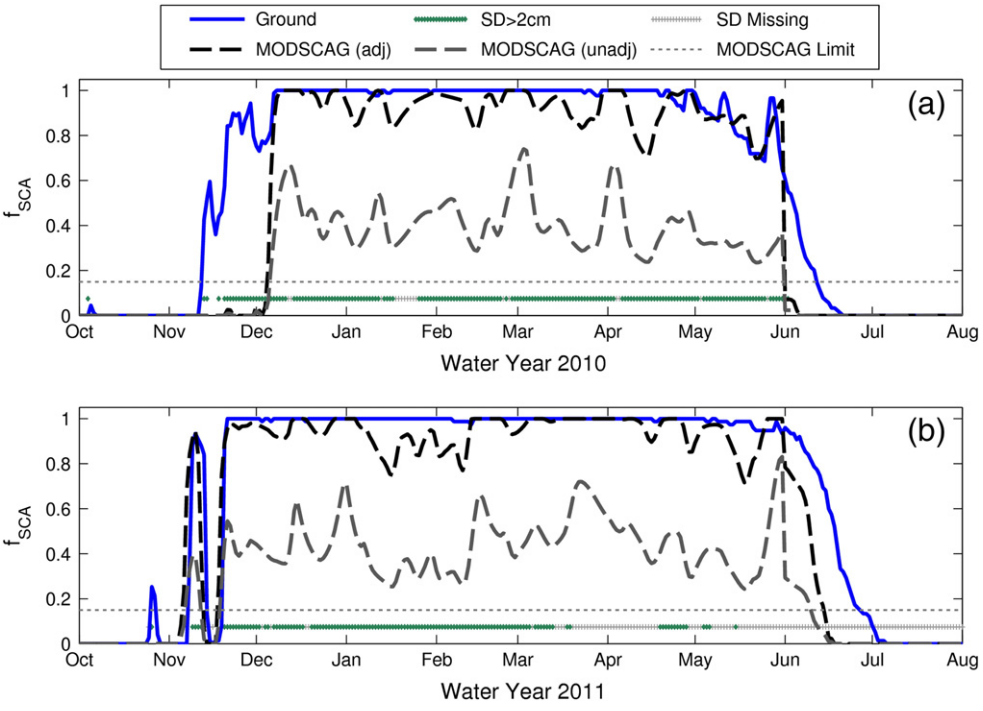

Fig. 9. Same as Fig. 8, except at the Onion Creek Experimental Forest (ONN), and with periods shown when snow depth (SD) exceeded 2 cm during 2010 and 2011. Most snow depth measurements were unavailable after March 2011 when the snow depth sensor arm was bent by heavy snow accumulation.

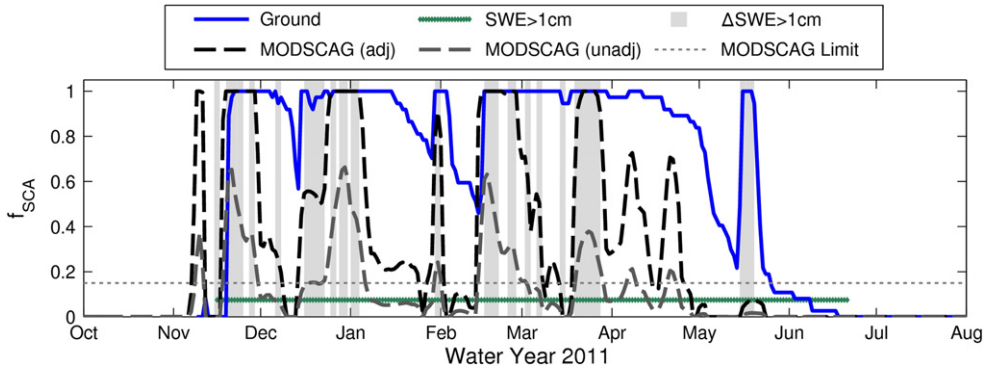

Fig. 10. Same as Fig. 8, except at the Yosemite Forest Dynamics Plot (YFDP) and during water year 2011 only. SWE values are taken from the Gin Flat snow pillow, 4 km from YFDP and 300 m higher in elevation. The shaded regions indicate periods when new SWE accumulation exceed 1 cm. Also shown are periods when the Gin Flat snow pillow reported snow presence (SWE > 1 cm). Note that the ground sensors did not begin recording data until 9 November 2010, so the first snow storm reported by MODSCAG was not evaluated.

during the two study years (Fig. 1). We investigated several possible reasons for this. First, it was possible that the ground sensor sampling strategy (Section 3.1) partially caused this difference, as sensors were not placed at potentially snow-free locations (e.g., rock outcroppings and open water). However, these features covered a small fraction (generally <0.05) of the land cover at each site. Second, this difference may have resulted from a documented underestimation bias in the NLCD forest cover dataset, which has been reported at 9.7% across the USA (Greenfield et al., 2009) and 23.4% in the Sierra Nevada zone (Nowak & Greenfield, 2010). However, by checking the NLCD forest cover against lidar-derived forest cover at TUM and YFDP, we found that the difference between NLCD forest cover and lidar forest cover was generally less than 5% at our sites. The mean f_{SCA} bias ranged from −0.14 to −0.24 during the winter at TUM and DAN (Fig. 11b), and therefore neither the sampling strategy nor the possible NLCD bias provides complete explanations for the difference between MODSCAG f_{SCA} and ground f_{SCA}.

We hypothesize that the use of static forest cover data to adjust for canopy (Eq. 2) was the primary cause of the MODSCAG f_{SCA} underestimation bias during the winter. Because canopy-adjusted MODSCAG f_{SCA} oscillated to values as high as 0.95 and 0.96 during the winter at TUM and DAN, respectively, this suggested that the canopy adjustment was effective over specific periods with favorable view angles and cloud conditions. MODIS band reflectance and viewable gap fraction (i.e., forest cover fraction) both change with view zenith angle, which changes daily for MODIS (Liu et al., 2008; Xin et al., 2012). While MODSCAG accounts for the view angle-dependent changes in surface reflectance, the static canopy adjustment used here did not account for the variation of viewable gap fraction with view angle. Therefore, the static adjustment may not be appropriate for adjusting f_{SCA} from scanning sensors (e.g., MODIS). Concurrent estimates of fractional vegetation from MODSCAG that account for the changing view angle, larger pixel size, and different reflectance would likely provide superior snow maps. More work is needed to determine whether a view angle dependent forest cover fraction improves canopy adjustments.

Canopy-adjusted MODSCAG also exhibited a fundamental limitation in that no snow cover was mapped once ground f_{SCA} approached the forest cover fraction (Fig. 7c, d). This problem cannot be corrected with the current adjustment method (Eq. 2), as $f_{SCA,obs}$ was 0 in these cases, inevitably resulting in $f_{SCA,adjusted}$ of 0, regardless of the forest cover value (f_{can}). This remains an outstanding challenge for satellite remote sensing of snow in forested areas.

The prevalence of omission errors (Table 2) at the forest sites (ONN and YFDP) and the inability of MODSCAG to map snow below the forest cover fraction (Fig. 7c, d) suggested that snow persisted longer under the canopy than in the viewable gaps and clearings at these two sites. Snow lasted 12 to 30 days longer at the ground networks of the forest sites (Figs. 9, 10) relative to MODSCAG snow cover. This difference in snow persistence in forests vs. clearings was consistent with other studies in the Sierra Nevada. Anderson (1956) found that snow cover disappeared in a dense forest 16 days after snow in large forest openings near ONN, while Church (1914) noted that snow persisted at least 7 to 10 days longer in pine and fir forests than treeless meadows near Lake Tahoe. These studies provide confidence in our observations, but we recognize that these results cannot be generalized for all forests, as forest characteristics (e.g., canopy structure, species, age) interact with snow in complex ways, resulting in variability of snow persistence (Kittredge, 1953). Nevertheless, we note that errors in snow disappearance timing

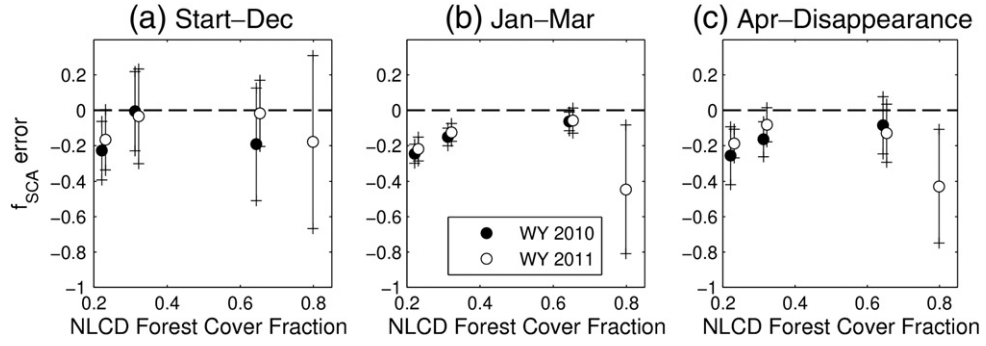

Fig. 11. Daily errors in canopy-adjusted MODSCAG f_{SCA} during water years 2010 and 2011 versus mean NLCD forest cover during (a) the early accumulation season (Start–Dec), (b) winter (Jan–Mar), and (c) the ablation season (Apr–Disappearance). The starting date in (a) was the first day with $f_{SCA} \geq 0.15$, while the disappearance date in (c) was the last day when $f_{SCA} \geq 0.15$. Mean errors are denoted by a circle and whiskers indicate 1 standard deviation from the mean error. The markers were displaced horizontally so the two water years could be shown without overlap at each site. The four sites listed in increasing forest cover are TUM, DAN, ONN, and YFDP.

impact applications such as SWE reconstruction. An error of 12 days in point snow disappearance has a potential error of 50% in reconstructed peak SWE, assuming a mean SWE error of 4.3% per day of snow disappearance date bias (Raleigh & Lundquist, 2012). Slater et al. (2012) show similar median SWE errors given ± 10 days uncertainty in snow disappearance.

We also note that the operational snow depth and SWE sensors in clearings at our study areas did not reliably represent snow disappearance timing in the adjacent forests, and these sensors have had wide usage in prior MODIS validation studies. Taking $f_{SCA}<0.15$ for snow absence, the timing of snow disappearance in 2010 from MODSCAG was within 2 days of observations at the operational snow sensors at TUM (Fig. 6a) and ONN (Fig. 9a). However, our ground temperature networks indicated that as much as 60% (ONN) to 84% (TUM) of the land was still snow-covered once snow disappeared at the operational sensors in 2010. In these cases, MODSCAG errors in snow disappearance were actually larger than the errors suggested by the operational data. We also observed cases when the operational snow sensors overestimated the MODSCAG errors in snow disappearance timing. For example, the DAN snow pillow data suggested that MODSCAG had a 7 day error in snow disappearance date in 2011 (Fig. 8b), but our ground-based sensors showed that MODSCAG only had a 2 day error. Thus, the issue of snow sensor representativeness (Rice & Bales, 2008) is critically important for comparisons between a MODIS pixel and a single snow sensor in that pixel. Because most snow pillows were positioned to provide streamflow indices (Farnes, 1967) and not to represent the timing and duration of snow presence of an area, we conclude that a single snow depth or SWE sensor cannot validate a MODIS pixel with confidence, especially in forested pixels. This has direct implications for prior studies that have used single snow sensors to validate MODIS.

While MODSCAG is more accurate than empirical MODIS snow cover retrievals early in the accumulation season and late in the ablation season (Rittger et al., 2012), our results show that MODSCAG errors are often most variable during these periods (Fig. 11a, c). This implies that intensive field surveys conducted near peak accumulation (e.g., CLPX) do not sample the largest MODIS snow cover errors in the seasonal snow zone. As suggested by the results at YFDP, large MODIS errors are expected to occur frequently in the transient snow zone where snow may accumulate and disappear multiple times in a single snow season. These difficulties support the use of distributed ground-based sensors to test MODIS snow cover, such as networks of ground temperature sensors (as in this study) or snow depth sensors (Musselman et al., 2012; Varhola et al., 2010b). Lidar observations of snow cover (e.g., Deems et al., 2006) may also test MODIS errors in forests, but the tradeoffs between timing, frequency, and costs of lidar flights must be considered carefully.

Although our sample size ($n=7$ site years) is relatively small considering the large variability in forest cover across the globe, we have (1) demonstrated a new methodology for ground validation of MODIS and (2) identified errors in forests that cannot be detected with previously used validation techniques (e.g., comparisons with Landsat and SNOTEL). Thus our results provide a first quantification of forest effects on f_{SCA} errors and highlight the need for continued testing of MODSCAG and canopy adjustment methods over a more complete range of forest cover and environmental conditions. This in turn will benefit users of MODSCAG for distributed applications, such as SWE reconstruction and snow model testing.

Acknowledgments

The authors thank Laura Hinkelman, Tom Ackerman, Janneke Hille Ris Lambers, Jeff Deems, Van Kane, and the Lundquist Mountain Hydrology group for the review and discussions that improved this paper. Thanks also to Dr. Marvin Bauer and three anonymous reviewers for the critical review. We would like to recognize Nic Wayand for field assistance, and Randall Osterhuber and Peggy Moore for arranging accommodations for field work at Onion Creek and Yosemite, respectively. M. Raleigh was supported by NASA Headquarters under the NASA Earth and Space Science Fellowship Program — Grant NNX09AO22H. K. Rittger was also supported by NASA Headquarters under the NASA Earth and Space Science Fellowship Program — Grant NNX09AN75H. This publication was partially funded by the Joint Institute for the Study of the Atmosphere and Ocean (JISAO) under NOAA Cooperative Agreement NA10OAR4320148, Contribution No. 7436, in association with the NOAA Hydrometeorological Testbed Project. Partial funding for J.A. Lutz and J.D. Lundquist was provided by NSF under grant number CBET-0931780.

References

Anderson, H. (1956). Forest-cover effects on snowpack accumulation and melt Central Sierra snow laboratory. *Transactions of the American Geophysical Union*, *37*(3), 307–312.

Baker, F. S. (1944). Mountain climates of the western United States. *Ecological Monographs*, *14*(2), 223–254.

Bormann, K. J., McCabe, M. F., & Evans, J. P. (2012). Satellite based observations for seasonal snow cover detection and characterisation in Australia. *Remote Sensing of Environment*, *123*, 57–71. http://dx.doi.org/10.1016/j.rse.2012.03.003.

Brubaker, K. L., Pinker, R. T., & Deviatova, E. (2005). Evaluation and comparison of MODIS and IMS snow-cover estimates for the Continental United States using station data. *Journal of Hydrometeorology*, *6*(6), 1002–1017. http://dx.doi.org/10.1175/JHM447.1.

Church, J. E. (1914). Recent studies of snow in the United States. *The Quarterly Journal of the Royal Meteorological Society*, *40*(169), 43–52.

Cline, D., Elder, K., Davis, R. E., Hardy, J. P., Liston, G. E., Imel, D., et al. (2003). Overview of the NASA cold land processes field experiment (CLPX-2002). *Proceedings of SPIE*, *4894*, 361–372. http://dx.doi.org/10.1117/12.467766.

Daly, C., Halbleib, M., Smith, J. I., Gibson, W. P., Doggett, M. K., Taylor, G. H., et al. (2008). Physiographically sensitive mapping of climatological temperature and precipitation across the conterminous United States. *International Journal of Climatology*, *28*(15), 2031–2064. http://dx.doi.org/10.1002/joc.1688.

Daly, C., Neilson, R. P., & Phillips, D. L. (1994). A statistical–topographic model for mapping climatological precipitation over mountainous terrain. *Journal of Applied Meteorology*, *33*, 140–158.

Deems, J. S., Fassnacht, S. R., & Elder, K. J. (2006). Fractal distribution of snow depth from LiDAR data. *Journal of Hydrometeorology*, *7*, 285–297.

Dong, J., & Peters-Lidard, C. (2010). On the relationship between temperature and MODIS snow cover retrieval errors in the western U.S. *IEEE Journal of Selected Topics in Applied Earth Observations and Remote Sensing*, *3*(1), 132–140. http://dx.doi.org/10.1109/JSTARS.2009.2039698.

Dozier, J. (1984). Snow reflectance from Landsat-4 thematic mapper. *IEEE Transactions on Geoscience and Remote Sensing*, *3*, 323–328.

Dozier, J., & Frew, J. (2009). Computational provenance in hydrologic science: A snow mapping example. *Philosophical Transactions. Series A, Mathematical, Physical, and Engineering Sciences*, *367*(1890), 1021-33. http://dx.doi.org/10.1098/rsta.2008.0187.

Dozier, J., Painter, T. H., Rittger, K., & Frew, J. (2008). Time–space continuity of daily maps of fractional snow cover and albedo from MODIS. *Advances in Water Resources*, *31*(11), 1515–1526. http://dx.doi.org/10.1016/j.advwatres.2008.08.011.

Durand, M., Molotch, N. P., & Margulis, S. A. (2008). Merging complementary remote sensing datasets in the context of snow water equivalent reconstruction. *Remote Sensing of Environment*, *112*(3), 1212–1225. http://dx.doi.org/10.1016/j.rse.2007.08.010.

Elder, K., Cline, D., Liston, G. E., & Armstrong, R. (2009). NASA cold land processes experiment (CLPX 2002/03): Field measurements of snowpack properties and soil moisture. *Journal of Hydrometeorology*, *10*(1), 320–329. http://dx.doi.org/10.1175/2008JHM877.1.

Farnes, P. (1967). Criteria for determining mountain snow pillow sites. *Proc. 35th western snow conf. Boise, Idaho* (pp. 59–62).

Greenfield, E., Nowak, D., & Walton, J. (2009). Assessment of 2001 NLCD percent tree and impervious cover estimates. *Photogrammetric Engineering and Remote Sensing*, *75*(11), 1279–1286.

Hall, D., Foster, J., Chang, A., Benson, C., & Chien, J. Y. L. (1998). Determination of snow-covered area in different land covers in central Alaska, USA, from aircraft data—April 1995. *Annals of Glaciology*, *26*, 149–155.

Hall, D., Foster, J., & Salomonson, V. (2001). Development of a technique to assess snow-cover mapping errors from space. *Geoscience and Remote Sensing*, *39*(2), 432–438.

Hall, D. K., Riggs, G. a, & Salomonson, V. V. (1995). Development of methods for mapping global snow cover using moderate resolution imaging spectroradiometer data. *Remote Sensing of Environment*, *54*(2), 127–140. http://dx.doi.org/10.1016/0034-4257(95)00137-P.

Hall, D. K., Riggs, G. A., Salomonson, V. V., DiGirolamo, N. E., & Bayr, K. J. (2002). MODIS snow-cover products. *Remote Sensing of Environment*, *83*(1–2), 181–194. http://dx.doi.org/10.1016/S0034-4257(02)00095-0.

Hall, D., Tait, A., Foster, J., Chang, A., & Allen, M. (2000). Intercomparison of satellite-derived snow-cover maps. *Annals of Glaciology*, *31*(1), 369–376.

Homan, J. W., Luce, C. H., McNamara, J. P., & Glenn, N. F. (2010). Improvement of distributed snowmelt energy balance modeling with MODIS-based NDSI-derived

fractional snow-covered area data. *Hydrological Processes*, *25*(4), 650–660. http://dx.doi.org/10.1002/hyp. 7857.
Homer, C., Huang, C., Yang, L., Wylie, B., & Coan, M. (2004). Development of a 2001 national land-cover database for the United States. *Photogrammetric Engineering and Remote Sensing*, *70*(7), 829–840.
Jost, G., Weiler, M., Gluns, D. R., & Alila, Y. (2007). The influence of forest and topography on snow accumulation and melt at the watershed-scale. *Journal of Hydrology*, *347*(1–2), 101–115. http://dx.doi.org/10.1016/j.jhydrol.2007.09.006.
Kane, V. R., Gillespie, A., McGaughey, R., Lutz, J. A., Ceder, K., & Franklin, J. F. (2008). Interpretation and topographic compensation of conifer canopy self-shadowing. *Remote Sensing of Environment*, *112*(10), 3820–3832. http://dx.doi.org/10.1016/j.rse.2008.06.001.
Kittredge, J. (1953). Influences of forests on snow in the Ponderosa, Sugar Pine, Fir Zone of the Central Sierra Nevada. *Hilgardia*, *22*, 1–96.
Klein, A., & Barnett, A. (2003). Validation of daily MODIS snow cover maps of the Upper Rio Grande River Basin for the 2000–2001 snow year. *Remote Sensing of Environment*, *86*(2), 162–176. http://dx.doi.org/10.1016/S0034-4257(03)00097-X.
Klein, A. G., Hall, D. K., & Riggs, G. A. (1998). Improving snow cover mapping in forests through the use of a canopy reflectance model. *Hydrological Processes*, *12*, 1723–1744.
Liang, T., Huang, X., Wu, C., Liu, X., Li, W., Guo, Z., et al. (2008). An application of MODIS data to snow cover monitoring in a pastoral area: A case study in Northern Xinjiang, China. *Remote Sensing of Environment*, *112*(4), 1514–1526. http://dx.doi.org/10.1016/j.rse.2007.06.001.
Liu, J., Melloh, R. A., Woodcock, C. E., Davis, R. E., & Ochs, E. S. (2004). The effect of viewing geometry and topography on viewable gap fractions through forest canopies. *Hydrological Processes*, *18*(18), 3595–3607.
Liu, J., Woodcock, C. E., Melloh, R. A., Davis, R. E., McKenzie, C., & Painter, T. H. (2008). Modeling the view angle dependence of gap fractions in forest canopies: Implications for mapping fractional snow cover using optical remote sensing. *Journal of Hydrometeorology*, *9*(5), 1005–1019. http://dx.doi.org/10.1175/2008JHM866.1.
Lundquist, J. D., & Lott, F. (2008). Using inexpensive temperature sensors to monitor the duration and heterogeneity of snow-covered areas. *Water Resources Research*, *44*, 8–13. http://dx.doi.org/10.1029/2008WR007035.
Lutz, J. A., Larson, A. J., Swanson, M. E., & Freund, J. A. (2012). Ecological importance of large-diameter trees in a temperate mixed-conifer forest. *PLoS One*, *7*(5), 1–15. http://dx.doi.org/10.1371/journal.pone.0036131.
Maurer, E. P., Rhoads, J. D., Dubayah, R. O., & Lettenmaier, D. P. (2003). Evaluation of the snow-covered area data product from MODIS. *Hydrological Processes*, *17*(1), 59–71. http://dx.doi.org/10.1002/hyp. 1193.
McGuire, M., Wood, A. W., Hamlet, A. F., & Lettenmaier, D. P. (2006). Use of satellite data for streamflow and reservoir storage forecasts in the Snake River basin. *Journal of Water Resources Planning and Management*, *132*(2), 97. http://dx.doi.org/10.1061/(ASCE)0733-9496(2006) 132:2(97).
Molotch, N. P., & Margulis, S. A. (2008). Estimating the distribution of snow water equivalent using remotely sensed snow cover data and a spatially distributed snowmelt model: A multi-resolution, multi-sensor comparison. *Advances in Water Resources*, *31*(11), 1503–1514. http://dx.doi.org/10.1016/j.advwatres.2008.07.017.
Musselman, K. N., Molotch, N. P., Margulis, S. A., Kirchner, P. B., & Bales, R. C. (2012). Influence of canopy structure and direct beam solar irradiance on snowmelt rates in a mixed conifer forest. *Agricultural and Forest Meteorology*, *161*, 46–56. http://dx.doi.org/10.1016/j.agrformet.2012.03.011.
National Aeronautics and Space Administration (NASA). (2001). *Landsat 7 science data users' handbook*. (Greenbelt, MD, USA).
Nolin, A. W. (2010). Recent advances in remote sensing of seasonal snow. *Journal of Glaciology*, *56*(200), 1141–1150.
Nowak, D. J., & Greenfield, E. J. (2010). Evaluating the national land cover database tree canopy and impervious cover estimates across the conterminous United States: A comparison with photo-interpreted estimates. *Environmental Management*, *46*(3), 378–390. http://dx.doi.org/10.1007/s00267-010-9536-9.
Painter, T. H., Rittger, K., McKenzie, C., Slaughter, P., Davis, R. E., & Dozier, J. (2009). Retrieval of subpixel snow covered area, grain size, and albedo from MODIS. *Remote Sensing of Environment*, *113*(4), 868–879. http://dx.doi.org/10.1016/j.rse.2009.01.001.
Parajka, J., & Blöschl, G. (2008). Spatio-temporal combination of MODIS images — Potential for snow cover mapping. *Water Resources Research*, *44*(3), 1–13. http://dx.doi.org/10.1029/2007WR006204.
Parajka, J., Haas, P., Kirnbauer, R., Jansa, J., & Blöschl, G. (2012). Potential of time-lapse photography of snow for hydrological purposes at the small catchment scale. *Hydrological Processes*. http://dx.doi.org/10.1002/hyp. 8389.
Pomeroy, J., & Granger, R. (1997). Sustainability of the western Canadian boreal forest under changing hydrological conditions. I. Snow accumulation and ablation. In D. Rosbjerg, B. Nour-Eddine, A. Gustard, Z. Kundzewics, & P. Rasmussen (Eds.), *Sustainability of water resources under increasing uncertainty (IAHS Publ 240)* (pp. 237–242). Wallingford: IAHS Press.
Pu, Z., Xu, L., & Salomonson, V. V. (2007). MODIS/Terra observed seasonal variations of snow cover over the Tibetan Plateau. *Geophysical Research Letters*, *34*(6), 1–6. http://dx.doi.org/10.1029/2007GL029262.
Raleigh, M. S., & Lundquist, J. D. (2012). Comparing and combining SWE estimates from the SNOW-17 model using PRISM and SWE reconstruction. *Water Resources Research*, *48*(1), 1–16. http://dx.doi.org/10.1029/2011WR010542.
Ralph, F. M., Rauber, R. M., Jewett, B. F., Kingsmill, D. E., Pisano, P., Pugner, P., et al. (2005). Improving short-term (0–48 h) cool-season quantitative precipitation forecasting: Recommendations from a USWRP workshop. *Bulletin of the American Meteorological Society*, *86*(11), 1619–1632. http://dx.doi.org/10.1175/BAMS-86-11-1619.
Rice, R., & Bales, R. (2008). Embedded sensor network design for spatial snowcover. *Proc. 76th western snow conference. Hood River, Oregon* (pp. 35–46).
Rice, R., Bales, R. C., Painter, T. H., & Dozier, J. (2011). Snow water equivalent along elevation gradients in the Merced and Tuolumne River basins of the Sierra Nevada. *Water Resources Research*, *47*(8), 1–11. http://dx.doi.org/10.1029/2010WR009278.
Richards, L. (1959). Forest densities, ground cover, and slopes in the snow zone of the Sierra Nevada west-side. *Technical papers. Pacific southwest forest and range experiment station*, *40*. (pp. 1–21).
Rittger, K., Kahl, A., & Dozier, J. (2011). Topographic distribution of snow water equivalent in the Sierra Nevada. *Proc. 79th western snow conf. Stateline, Nevada* (pp. 37–46).
Rittger, K., Painter, T. H., & Dozier, J. (2012). Assessment of methods for mapping snow cover from MODIS. *Advances in Water Resources*. http://dx.doi.org/10.1016/j.advwatres.2012.03.002.
Serreze, M. C., Clark, M. P., Armstrong, R. L., McGinnis, D. A., & Pulwarty, R. S. (1999). Characteristics of the western United States snowpack from snowpack telemetry (SNOTEL) data. *Water Resources Research*, *35*(7), 2145. http://dx.doi.org/10.1029/1999WR900090.
Shamir, E., & Georgakakos, K. P. (2006). Distributed snow accumulation and ablation modeling in the American River basin. *Advances in Water Resources*, *29*(4), 558–570. http://dx.doi.org/10.1016/j.advwatres.2005.06.010.
Simic, A., Fernandes, R., Brown, R., Romanov, P., & Park, W. (2004). Validation of VEGETATION, MODIS, and GOES + SSM/I snow-cover products over Canada based on surface snow depth observations. *Hydrological Processes*, *18*(6), 1089–1104. http://dx.doi.org/10.1002/hyp. 5509.
Slater, A. G., Barrett, A. P., Clark, M. P., Lundquist, J. D., & Raleigh, M. S. (2012). Uncertainty in seasonal snow reconstruction: Relative impacts of model forcing and image availability. *Advances in Water Resources*. http://dx.doi.org/10.1016/j.advwatres.2012.07.006.
Storck, P., Lettenmaier, D., & Bolton, S. (2002). Measurement of snow interception and canopy effects on snow accumulation and melt in a mountainous maritime climate, Oregon, United States. *Water Resources Research*, *38*(11), 1–16.
Tan, B., Woodcock, C. E., Hu, J., Zhang, P., Ozdogan, M., Huang, D., et al. (2006). The impact of gridding artifacts on the local spatial properties of MODIS data: Implications for validation, compositing, and band-to-band registration across resolutions. *Remote Sensing of Environment*, *105*(2), 98–114. http://dx.doi.org/10.1016/j.rse.2006.06.008.
Tekeli, A. E., Akyürek, Z., Arda Şorman, A., Şensoy, A., & Ünal Şorman, A. (2005). Using MODIS snow cover maps in modeling snowmelt runoff process in the eastern part of Turkey. *Remote Sensing of Environment*, *97*(2), 216–230. http://dx.doi.org/10.1016/j.rse.2005.03.013.
Tyler, S. W., Burak, S. A., McNamara, J. P., Lamontagne, A., Selker, J. S., & Dozier, J. (2008). Spatially distributed temperatures at the base of two mountain snowpacks measured with fiber-optic sensors. *Journal of Glaciology*, *54*(187), 673–679.
USGS (2011). Seamless data warehouse. (Retrieved October 20, 2011, http://seamless.usgs.gov/
Varhola, A., Coops, N. C., Weiler, M., & Moore, R. D. (2010). Forest canopy effects on snow accumulation and ablation: An integrative review of empirical results. *Journal of Hydrology*, *392*(3–4), 219–233. http://dx.doi.org/10.1016/j.jhydrol.2010.08.009.
Varhola, A., Wawerla, J., Weiler, M., Coops, N. C., Bewley, D., & Alila, Y. (2010). A new low-cost, stand-alone sensor system for snow monitoring. *Journal of Atmospheric and Oceanic Technology*, *27*(12), 1973–1978. http://dx.doi.org/10.1175/2010JTECHA1508.1.
Vikhamar, D., & Solberg, R. (2003). Snow-cover mapping in forests by constrained linear spectral unmixing of MODIS data. *Remote Sensing of Environment*, *88*(3), 309–323. http://dx.doi.org/10.1016/j.rse.2003.06.004.
Vogel, S. W. (2002). Usage of high-resolution Landsat 7 band 8 for single-band snow-cover classification. *Annals of Glaciology*, *34*(1), 53–57. http://dx.doi.org/10.3189/172756402781818058.
Wall, M., Rechtsteiner, A., & Rocha, L. M. (2003). Singular value decomposition and principal component analysis. In D. P. Berrar, W. Dubitzky, & M. Granzow (Eds.), *A practical approach to microarray data analysis* (pp. 91–109). Norwell, MA: Kluwer.
Wiscombe, W., & Warren, S. (1980). A model for the spectral albedo of snow. I: Pure snow. *Journal of the Atmospheric Sciences*, *37*, 2712–2733. http://dx.doi.org/10.1175/1520-0469(1980) 037<2712:AMFTSA>2.0.CO;2.
Xin, Q., Woodcock, C. E., Liu, J., Tan, B., Melloh, R. a, & Davis, R. E. (2012). View angle effects on MODIS snow mapping in forests. *Remote Sensing of Environment*, *118*, 50–59. http://dx.doi.org/10.1016/j.rse.2011.10.029.
Yamaguchi, Y., Kahle, A., Tsu, H., Kawakami, T., & Pniel, M. (1998). Overview of advanced spaceborne thermal emission and reflection radiometer (ASTER). *IEEE Transactions on Geoscience and Remote Sensing*, *36*(4), 1062–1071. http://dx.doi.org/10.1109/36.700991.
Young, C. A., Escobar-Arias, M. I., Fernandes, M., Joyce, B., Kiparsky, M., Mount, J. F., et al. (2009). Modeling the hydrology of climate change in California's Sierra Nevada for subwatershed scale adaptation. *JAWRA Journal of the American Water Resources Association*, *45*(6), 1409–1423. http://dx.doi.org/10.1111/j.1752-1688.2009.00375.x.
Zhou, X., Xie, H., & Hendrickx, J. M. H. (2005). Statistical evaluation of remotely sensed snow-cover products with constraints from streamflow and SNOTEL measurements. *Remote Sensing of Environment*, *94*(2), 214–231. http://dx.doi.org/10.1016/j.rse.2004.10.007.